ACS OMEGA

http://pubs.acs.org/journal/acsodf

Article

Nuclear Magnetic Resonance-Based Metabolomics Approach Revealed the Intervention Effect of Using Complementary and Alternative Medicine (CAM) by CKD Patients

Nikhil Gupta,[‖] Deependra Kumar Yadav,[‖] Sonam Gautam, Ashish Kumar, Dinesh Kumar,* and Narayan Prasad*

Cite This: *ACS Omega* 2023, 8, 7722−7737

Read Online

ACCESS | Metrics & More | Article Recommendations | Supporting Information

ABSTRACT: Chronic kidney disease (CKD) is the end point of a number of systemic chronic diseases. The prevalence of CKD is increasing worldwide and recent epidemiological studies are showing the high prevalence of renal failure in CKD patients using complementary and alternative medicines (CAMs). Clinicians believe that biochemical profiles of CKD patients using CAM (referred here to as CAM-CKD) may be different compared to those on standard clinical treatment and should be managed differently. The present study aims to explore the potential of the NMR-based metabolomics approach to reveal the serum metabolic disparity between CKD and CAM-CKD patients with respect to normal control (NC) subjects and if the differential metabolic patterns can provide rationale for the efficacy and safety of standard and/or alternative therapies. Serum samples were obtained from 30 CKD patients, 43 CAM-CKD patients, and 47 NC subjects. The quantitative serum metabolic profiles were measured using 1D ^{1}H CPMG NMR experiments performed at 800 MHz NMR spectrometer. The serum metabolic profiles were compared using various multivariate statistical analysis tools available on MetaboAnalyst (freely available web-based software) such as partial least-squares discriminant analysis (PLS-DA) and random forest (a machine learning) classification method. The discriminatory metabolites were identified based on variable importance in projection (VIP) statistics and further evaluated for statistical significance (i.e., $p < 0.05$) using either Student *t*-test or ANOVA statistics. PLS-DA models were capable of clustering CKD and CAM-CKD with considerably high values of Q^2 and R^2. Compared to CAM-CKD patients, the sera of CKD patients were characterized by (a) elevated levels of urea, creatinine, citrate, glucose, glycerol, and phenylalanine and phenylalanine-to-tyrosine ratio (PTR) and (b) decreased levels of various amino acids (such leucine, isoleucine, valine, and alanine), high-density lipoproteins, lactate, and acetate. These changes suggested that CKD patients manifest severe oxidative stress, hyperglycemia (with dampened glycolysis), increased protein energy wasting, and reduced lipid/membrane metabolism. Statistically significant and strong positive correlation of PTR with serum creatinine levels suggested the role of oxidative stress in the progression of kidney disease. Significant differences in metabolic patterns between CKD and CAM-CKD patients were observed. With respect to NC subjects, the serum metabolic changes were more aberrant in CKD patients compared to CAM-CKD patients. The aberrant metabolic changes in CKD patients with manifestations of higher oxidative stress compared to CAM-CKD patients could explain clinical discrepancies between CKD and CAM-CKD patients and further advocate the use of different treatment strategies for CKD and CAM-CKD patients.

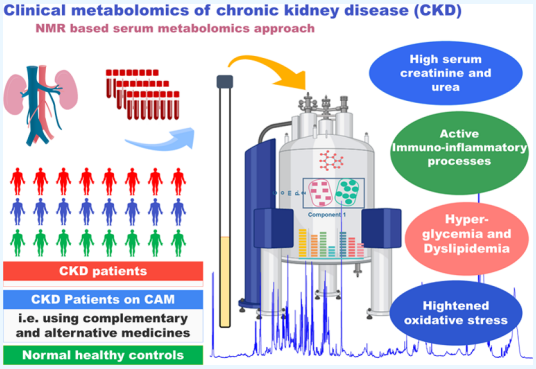

INTRODUCTION

Chronic kidney disease (CKD), an irreversible progressive renal function disorder, with an estimated worldwide prevalence of nearly 8−16%, is becoming a serious public health issue as its prevalence is increasing worldwide.[1−3] Worldwide, diabetes mellitus is the most common cause of CKD; however, other causes, such as herbal and environmental toxins, have been found to be more common in some regions.[3] CKD is often diagnosed quite late and a decrease in glomerular filtration rate (GFR) leads to serious mortality in many patients worldwide. Further, patients exhibit structural and/or functional abnormalities in kidneys (present for more than 3 months), causing a decreased renal function and altered metabolic activity of the kidney. Clinically, CKD is defined as a reduced glomerular filtration rate, increased urinary albumin excretion, or both, which may also occur as a result of uncontrolled/complicated

Received: November 17, 2022
Accepted: January 26, 2023
Published: February 16, 2023

https://doi.org/10.1021/acsomega.2c06469
ACS Omega 2023, 8, 7722−7737

Table 1. Clinical and Demographic Characteristics of Subjects Included in the Study[a]

	CKD (N = 30)	CAM-CKD (N = 43)	CAM-CKD (N = 26)[b]	normal control (N = 47)
male (female)	25 (5)	35 (08)	16 (10)	40 (7)
mean age ± standard deviation	43.3 ± 14.9	49.4 ± 11.36	49.7 ± 15.0	47.4 ± 8.1
staging (I, II, III, IV, V)	3, 3, 2, 5, 17	3, 8, 12, 3, 7	3, 0, 7, 2, 10	
hemoglobin (g/dL)	9.01 ± 2.45	11.1 ± 2.22		
total leukocyte count (TLC, cells/mm^3)	7531.4 ± 3054.0	14069.4 ± 26496.6		
platelets (G/L)	144,469 ± 67,530	315,242.4 + 524,167.7		
serum creatinine (mg/dL)	5.91 ± 3.32	3.26 ± 3.22	4.90 ± 3.55	
eGFR (mL/min)	24.2 ± 27.0	43.5 ± 30.0	31.7 ± 33.2	
serum albumin (g/dL)	3.72 ± 0.47	3.85 ± 0.57		
serum sodium (meq/L)	133.67 ± 6.08	140.44 ± 3.77		
serum potassium (meq/L)	4.90 ± 0.91	4.75 ± 0.57		

[a]Abbreviations used: meq/L, milliequivalents per liter; mg/dL, milligram per deciliter; mL, milliliter; G/L, Giga/liter; g/dL, gram per deciliter. [b]Validation cohort of 26 CAM-CKD patients. The clinical details (such as hemoglobin, total leukocyte count (TLC), platelets, serum albumin, serum sodium, and serum potassium) are not available.

metabolic disorder such as diabetes mellitus (DM), hypertension, liver diseases, or glomerulonephritis.[3,4] Although the estimated glomerular filtration rate (eGFR) and serum creatinine are routinely used for the assessment of CKD, however, these parameters may also depend on muscle metabolism and muscular activities and often lead to erroneous results for those who embody extremes of muscle mass such as bodybuilders and amputees and those with sarcopenia or other muscle-wasting disorders.[4] Therefore, investigating other diagnostic measures would be of immense value to aid in further understanding of the CKD onset, progression, and prognosis to offer more appropriate treatment for improved patient care.

The complementary and alternative medicine (CAM) has been used for thousands of year according to the theories, beliefs, and experiences that originated from different cultures and employed to keep health and prevent, diagnose, improve, or treat physical and mental illnesses.[2,5] A recent study reported that the utilization rate of CAM among patients with chronic diseases at outpatient clinics is about 63.9%.[6] The use of CAM is also widespread, including countries like India, and studies report that about 66% of CKD patients have been using some or the other form of CAM.[7,8] The use of CAM among CKD patients has been found to be high in the age range of 50−64 years (67%).[9] Clinicians believe that the disease mechanism and so biochemical profiles of CKD patients using standard clinical treatment may be different from those CKD patients using CAM (referred here to as CAM-CKD) for the management of systemic chronic diseases such as diabetes mellitus (DM), hypertension, glomerulonephritis, etc. The present study has been undertaken to probe this conjectureby making use of NMR-based clinical metabolomics approach. This is because CKD is commonly associated with specific changes in circulating metabolome and may involve metabolic comorbidities (e.g., diabetes mellitus, hypertension, hypercholesterolemia, fatty liver, obesity, or cardiovascular disease).[10] Serum metabolomics analysis is becoming an influential methodology for investigating metabolic biomarkers in chronic kidney disease (CKD) for diagnostic screening, predicting disease progression, and deciding the appropriate treatment.[4,11−17] The resulted metabolic disturbances associated with the severity of the disease mirror the phenotype of an organism and provide a detailed understanding of the metabolic processes involved in a disease.[18] The specific advantages of using NMR spectroscopy for metabolic analysis are that it is nondestructive (the sample analyzed can be used for further biochemical analysis), highly reproducible, inherently quantitative, and requiring minimal or no sample preparation.[19]

RESULTS

Patient Characteristics. The study involved 73 CKD patients and 47 normal control (NC) subjects. Depending upon the clinical history of CKD patients, i.e., if these patients have been using CAM for more than 3 months prior to the CKD diagnosis or not using CAM, these were categorized into two groups: CKD (not using CAMs, N = 30) and CAM-CKD (using CAMs, N = 43). The patient clinical and demographic details are listed in Table 1. The serum creatinine levels were used to estimate the glomerular filtration rate (eGFR) as described previously.[20−22] Following the criterion described previously,[23] five stages were defined for CKD patients corresponding to two groups of patients. For each patient group, the patient number in each CKD stage is plotted and the results are shown in the Supporting Information (Figure S1). It is clearly evident that patients in stage 5 are the maximum (N = 17) in the CKD group (N = 30), whereas those in stage 3 were found to be the maximum (N = 12) followed by stage 5 (n = 7) in the CAM-CKD group (see the Supporting Information, Figure S1). The different stages of a disease have heterogeneous metabolic alterations or metabolic homeostasis but have discrete underlying pathogenesis (pathobiology), rendering specific patterns of metabolic changes. The present study aims to identify these specific patterns of metabolic alternations in CKD and CAM-CKD patient groups.

Multivariate Statistical Analysis to Access the Metabolic Variations between CKD and CAM-CKD Groups. The 1D ^{1}H CPMG NMR spectra recorded at an 800 MHz NMR spectrometer have the potential to provide high-resolution metabolic snapshot and physiological patterns across diverse human serum samples. The cumulative 1D ^{1}H CPMG NMR spectra of serum samples obtained from CKD (in blue) and CAM-CKD (in red) patients are stacked and shown in the Supporting Information, Figure S2. Before starting the multivariate analysis based on NMR spectral features, the CPMG spectral peaks (and so the spectral regions) were assigned for specific serum metabolites, making composite use of the 800 MHz metabolite spectral database library of CHENOMX NMR suite. Some selected CPMG NMR spectra were opened in the processor module of CHENOMX software, manually phased, corrected for baseline distortions, and referenced with respect to

https://doi.org/10.1021/acsomega.2c06469
ACS Omega 2023, 8, 7722−7737

a singlet peak of formate (CH−) at δ(8.43 ppm). The processed CPMG NMR spectra were then opened into the profiler module of CHENOMX NMR suite, and the NMR peaks of various metabolites were identified and assigned by comparing and matching the chemical shift positioning, broadening, intensity, and *J*-coupling peak patterns with the spectral patterns of CHENOMX 800 MHz database metabolites. The 2D JRES spectrum was used to elucidate the *J*-coupled multiplicity of metabolite peaks in the CPMG NMR spectrum. The 2D ^{13}C HSQC spectrum and ^{1}H−^{1}H TOCSY spectra were analyzed using the semi-automated software program "MetaboMiner" to identify the metabolic peaks by comparing and matching the built-in metabolic library peak patterns. The assignment of NMR peaks in the spectral overlap regions and the NMR peaks of metabolites having singlet peaks in the ^{1}H NMR spectrum (such as glycine, acetate, acetone, TMAO, etc.) was further corroborated by their specific ^{13}C chemical shifts in the ^{13}C HSQC spectrum and peak at the zero line of the 2D JRES spectrum. The procedure provided us the assignment of (a) most of the amino acids such as alanine, glycine, glutamate, glutamine, proline, lysine, arginine, leucine, isoleucine, methionine, valine, serine, threonine, histidine, phenylalanine, and tyrosine, (b) metabolites of the glycolysis pathway (glucose, lactate, pyruvate, and citrate) along with some other metabolites like creatinine, acetate, 3-hydroxybutyrate (3HB), acetone, trimethylamine (TMA), trimethylamine-*N*-oxide (TMAO), and dimethyl-sulfone (DMS), and (c) lipid and membrane metabolites such as glycerol, choline, and glycerophosphocholine (GPC). The assignment of signals of high-density lipoproteins (HDL), low-density lipoproteins (LDL), very-low-density lipoproteins (VLDL), and polyunsaturated fatty acids (PUFAs) was based on previous reports. Although metabolic differences in the NMR spectra of study groups are often not compared visually, however, a visual comparison of spectral features clearly revealed that the serum creatinine levels are relatively elevated in the CKD group compared to the CAM-CKD group (Figure S2A,B). This observation was found to be well consistent with the clinically estimated serum creatinine levels in these two groups (see Figure S2C), suggesting that the acquired NMR spectra are manifesting clinically relevant information and are deemed appropriate for further comparison employing multivariate statistical data analysis tools.

First, the CPMG data matrix containing normalized spectral features was analyzed using the unsupervised principal component analysis (PCA) method for evaluating initial grouping trends and class separation. The PCA score plots showed a clear trend of group clustering and discrimination between the patients and NC cohorts but no evident discrimination between CKD and CAM-CKD patient cohorts. Two outliers were found in the CAM-CKD group and excluded from the analysis (one outlier spectrum was of the plasma sample and the other contained a broad signal at a chemical shift of 1.15 ppm and a bulged/distorted baseline near the water region from the 4.0 to 5.7 ppm region). Next, we used the supervised PLS-DA approach, and the resulted 2D and 3D score plots (see the Supporting Information, Figure S3A,B,B′) showed statistically significant separation between patient and NC groups with R2 and Q2 values close to 0.8, suggesting that the discriminatory model is adequately valid and can predict better than chance (see the Supporting Information, Figure S3C). However, separation between CKD and CAM-CKD patient groups was not evident. Further, we performed OPLS-DA to demonstrate the separation between study groups (CKD, CAM-CKD, and NC). The resulted 2D score plot (see the Supporting Information, Figure S3B) though clearly showed that patient groups are well separated from the NC group; however, the samples of CKD and CAM-CKD groups were found exquisitely overlapping (see the Supporting Information, Figure S3D). One predictive component (with R2X = 0.125, R2Y = 0.524, and Q2 = 0.495) and one orthogonal component (with R2X = 0.188, R2Y = 0.182, and Q2 = 0.106) were involved in the OPLS-DA model, which showed that the model had adequate stability (see the Supporting Information, Figure S3E). Further, VIP score plot analysis revealed more than 40 spectral features with VIP score > 1.0 (see the Supporting Information, Figure S3F), suggesting their discriminatory potential as per the VIP score indexing, i.e., the higher the VIP score, the higher the discriminatory potential of the metabolic feature in separating the study cohorts. The majority of discriminatory spectral features belonged to lipoproteins (such as HDL, LDL, and VLDL), lipid/membrane metabolites (such as choline, GPC, PUFA, etc.), and other abundantly present metabolites such as glucose, lactate, creatinine, alanine, and isoleucine (see the Supporting Information, Figure S3F). However, other serum metabolites present in relatively low abundance failed to mark their presence in the VIP score plot. This is because the 1D ^{1}H NMR spectrum of a serum sample often contains broad NMR signals [i.e., δ(0.76 to 0.96, 1.20 to 1.36, 1.92 to 2.04, 2.90 to 3.00, and 5.23 to 5.33 ppm)] corresponding to either lipoproteins and lipid/membrane metabolites in addition to dominant signals of metabolites present in large abundance (such as glucose and lactate). Another problem with this conventional procedure of analyzing all the spectral features (including those corresponding to blank/undesired spectral regions with no metabolic annotations), the dominant signals of lipoproteins (LDL and VLDL), lipid/membrane metabolites, and glucose, which contribute to multiple spectral bins, is that it does not render the subtle metabolic changes to mark their presence in the VIP score plot (as evident from Figure S3F in the Supporting Information). Therefore, we legitimately improved the relevant information content by (a) excluding the redundant spectral bins from the data matrix and combining some of the bins corresponding to a particular metabolite and (b) moreover screening discriminatory metabolites employing random forest (RF) classification, which is an advanced machine learning approach for supervised classification analysis and further considers the statistical significance while screening the features (biomarkers) of discriminatory potential from higher-dimensional metabolomics data.[24,25] Overall, a pruned data matrix containing 49 NMR spectral features (tabulated in Table S1 of the Supporting Information) was created and used further to perform multivariate discriminatory analysis for the identification of serum metabolic disturbances associated with CKD and CAM-CKD patients with respect to NC subjects. As oxidative stress is known to play an important role in the development and progression of CKD disease,[26−32] two additional spectral features (PTR1 and PTR2) representing the apparent phenylalanine-to-tyrosine ratio (PTR) (see the Supporting Information) were evaluated, and as per the details, they are described in the caption of Table S1 as well. The reason for this inclusion is that elevated PTR levels have been demonstrated to serve as indicative biomarkers of oxidative stress in different pathophysiological conditions.[33−37] After preparing the pruned data matrix containing adequate (total of 51) NMR spectral features, the RF classification models generated using complete and pruned data matrices were compared for their discriminatory

https://doi.org/10.1021/acsomega.2c06469
ACS Omega 2023, 8, 7722−7737

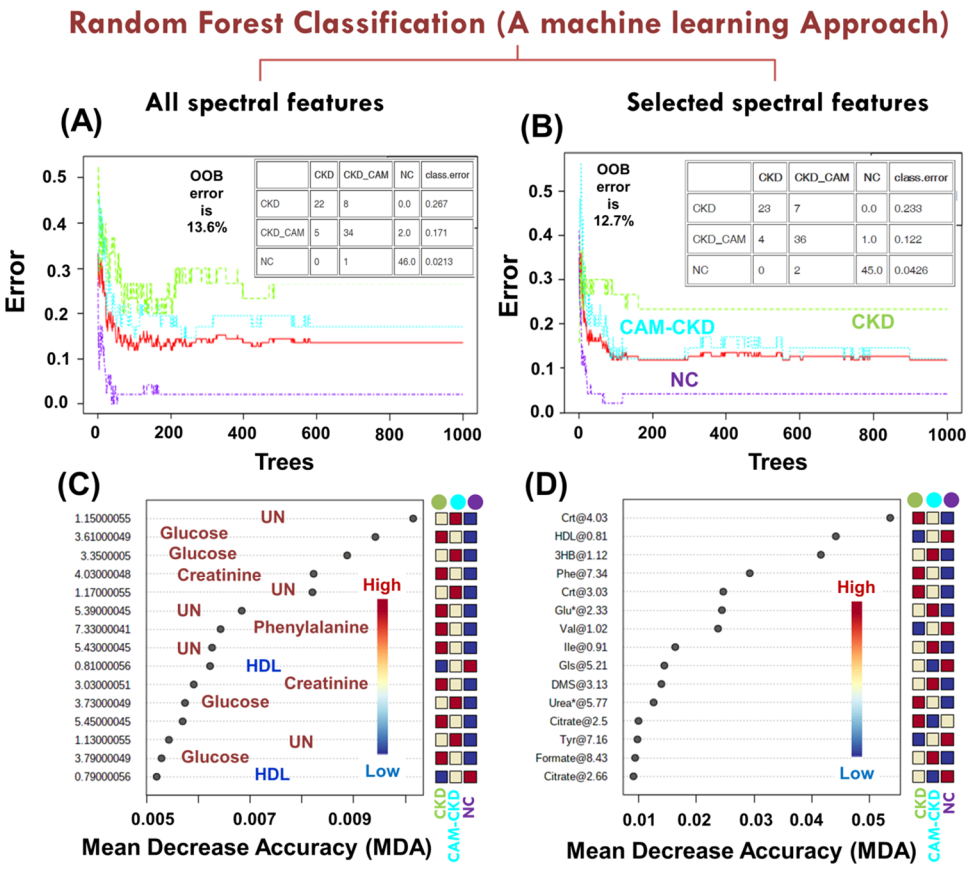

Figure 1. (A, B) Random forest (RF) classification models showing cumulative error rates measured for each class using the RF machine learning approach. (C, D) Significant features were identified by ranking of mean decrease accuracy (MDA) extracted with RF analysis when the features are permuted. The overall error rate is shown as the red line, and other color lines represent the error rates for each class as indicated. The out-of-bag (OOB) errors for the RF models generated (A, C) using all spectral features and (B, D) selected spectral features (as per the details provided in the Supporting Information, Table S1) were found to be 13.6 and 12.7%, respectively. Abbreviations used are as follows: Gls, glucose; Gln, glutamine; Glu, glutamate; Phe, phenylalanine; Tyr, tyrosine; His, histidine; 3HB, 3-hydroxybutyrate; Crt, creatinine; Ile, isoleucine; DMS, dimethyl-sulfone; Val, valine; HDL, high-density lipoproteins. As mentioned here, spectral bins with an asterisk "*" represent the cumulative signal of bins corresponding to the specified metabolite peak at that ppm. Bins specified by an even number for the last decimal place represent the cumulative signals of two adjacent bins, e.g., Tyr@7.16 represents the sum of Tyr@7.15 and Tyr@7.17 and like this for other such features.

performance as shown in Figure 1A,B. It is clearly evident that the serum metabolic profiles of CKD patients are distinctively different compared to CAM-CKD patients with respect to NC subjects (Figure 2A,B). The out-of-bag (OOB) error for the RF model based on all spectral features was found to be 13.6%, suggesting its high prediction accuracy, that is, 86.4% (Figure 2A). However, for the RF model based on discrete/selected spectral features, the out-of-bag (OOB) error was found to be improved further to 12.7%, suggesting its high prediction accuracy, that is, 87.3% (Figure 2A). Significant features were identified by ranking of mean decrease accuracy (MDA) extracted when the features are permuted, and the MDA score plots are shown in Figure 2C,D. It is clearly evident that there is high redundancy and the presence of unidentified features in the MDA plot derived from RF classification based on all spectral features (Figure 2C). On the other hand, the MDA plot derived from RF classification based on selected spectral features provided exquisite information about the metabolic alterations underlying the pathophysiology of the disease. The identified metabolic changes were further evaluated for statistical significance using the ANOVA approach, and the results are summarized in the Supporting Information (Table S2 and Figure S3). Compared to healthy normal control subjects, the CKD (including CAM-CKD) patients were characterized by (a) decreased serum levels of lipid and membrane metabolites (including HDL, LDL, VLDL, PUFA, choline, and GPC), the majority of amino acids (such as alanine, histidine, and glutamine), and *N*-acetylglycoproteins (NAGs) and (b) increased serum levels of creatinine, acetate, formate, *N*-alpha acetyl lysine (NAAL), various branched chain amino acids (such as isoleucine, leucine, and valine), glutamate, and phenylalanine and phenylalanine-to-tyrosine ratio (PTR). These changes are indicative of a state of chronic inflammation sustained through activated glutaminolysis and oxidative stress (as inferred from the elevated serum PTR levels).

Pairwise PLS-DA Analysis for Evaluating Serum Metabolic Disparity between Study Groups. The pruned CPMG data matrix was further used to perform pairwise PLS-DA analysis (Figure 2) and evaluate the extent of serum metabolic disparity between patient and NC groups. The key observations are summarized below:

(1) The serum metabolic profiles of CKD and CAM-CKD patients are distinctively different compared to NC subjects as inferred from exquisitely clustered and well-separated CKD and CAM-CKD samples from NC samples (Figure 2A,B).

https://doi.org/10.1021/acsomega.2c06469
ACS Omega 2023, 8, 7722−7737

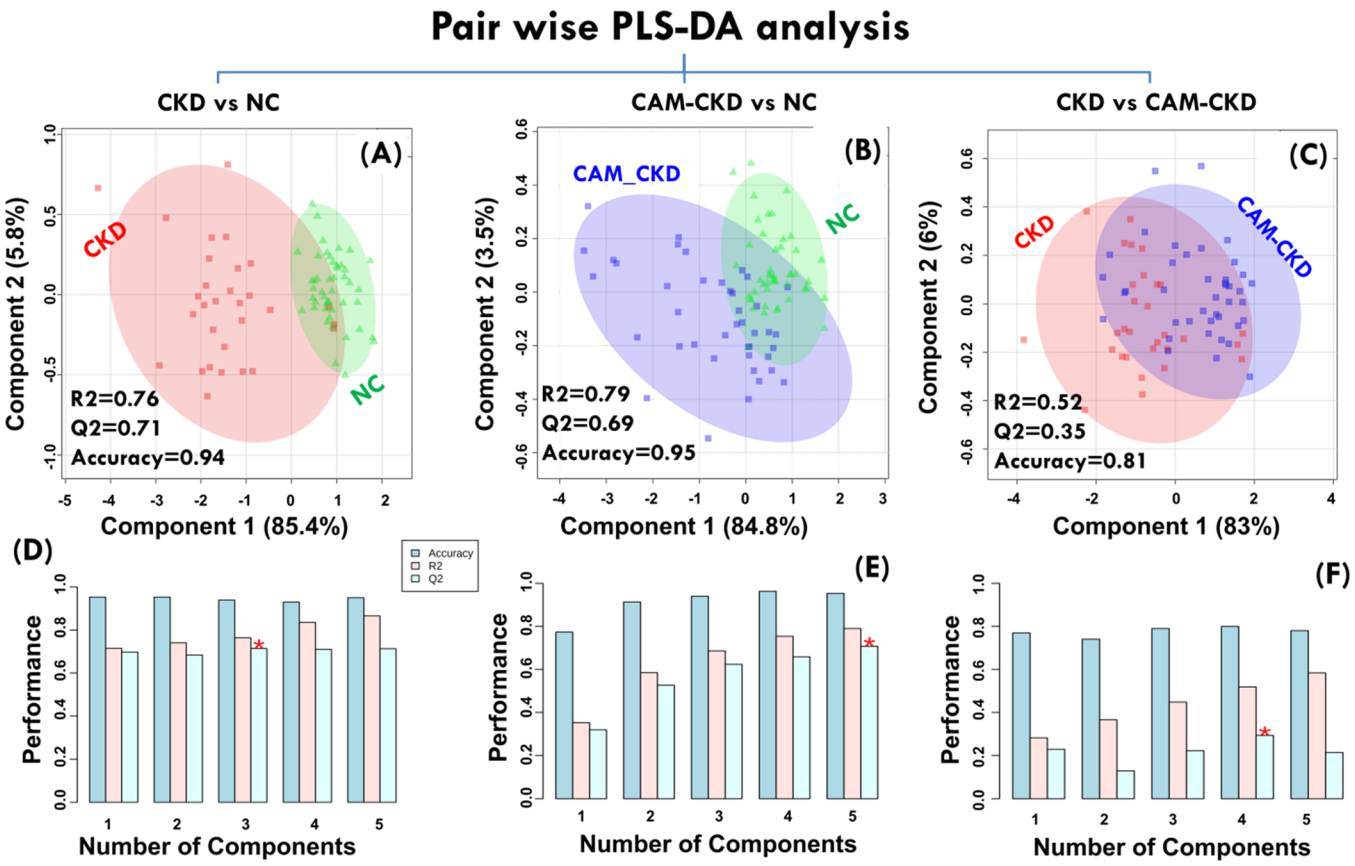

Figure 2. 2D score plots derived from the pairwise PLS-DA analysis of the pruned CPMG data matrix generated by selecting the spectral bins from the complete data matrix corresponding to various metabolites as listed in Table S1 of the Supporting Information: (A) CKD vs NC, (B) CAM-CKD vs NC, and (C) CKD vs CAM-CKD. The shaded or semitransparent areas represent the 95% confidence regions of each group as depicted by their respective colors. Abbreviations used here are as follows: CKD, chronic kidney disease; CAM-CKD, CKD patients practicing traditional complementary and alternative medicines; NC, normal control. (D−F) Bar plots showing the three performance measures (prediction accuracy, multiple correlation coefficient R^2, and explained variance in prediction Q^2) obtained after the 10-fold cross-validation analysis of multivariate data. The red star indicates the best classifier.

(2) The Q2 values for the discriminatory model between NC and CKD (highest Q2 = 0.71, Figure 2D) were found to be consistently higher compared to those for the discriminatory model between NC and CAM-CKD (highest Q2 = 0.69, Figure 2E), suggesting that the alterations in serum metabolic profiles are more aberrant in CKD patients compared to CAM-CKD patients with respect to NC subjects.

(3) The Q2 values for the discriminatory model between CKD and CAM-CKD were found to be positive but consistently lower (highest Q2 = 0.35, Figure 2F) compared to those for the discriminatory model between NC and patients (Figure 2D,E), suggesting that the use of CAM though has conferred legitimate serum metabolic changes; however, the metabolic disturbances are closely related in CKD and CAM-CKD patients owing to similar underlying pathophysiology.

Random Forest Classification Analysis to Access the Metabolic Variations between CKD and CAM-CKD Groups. The random forest (RF) classification analysis was further used to evaluate the serum metabolic disparity (a) between NC and diseased groups (Figure 3) and (b) between CKD and CAM-CKD groups (Figure 4). The RF models generated for comparison between CKD vs NC and CAM-CKD vs NC were found to be of high prediction accuracy, that is, more than 96% (Figure 3A,B), in good concordance with 10-fold cross-validation parameters of corresponding PLS-DA modeling (shown in Figure 2D,E). Discriminatory features were identified by ranking of mean decrease accuracy (MDA, Figure 3C,D) and checked for their statistical significance with the help of volcano plots (Figure 3E,F).

Random Forest Analysis to Access the Metabolic Variations between CKD and CAM-CKD Groups. The RF classification model was generated using selected spectral features, and the results are shown in Figure 4. The out-of-bag (OOB) error for the RF model was found to be 15.5%, suggesting its moderate prediction accuracy, that is, 84.5% (Figure 4A), in good concordance with 10-fold cross-validation parameters of corresponding PLS-DA modeling (shown in Figure 2F). The potential discriminatory metabolites were identified from the MDA plot derived from RF classification analysis (Figure 4B), and the statistical significance of key metabolic features was reconfirmed using the Student *t*-test (Figure 4C). Compared to those of CAM-CKD patients, the sera of CKD patients were characterized by (a) elevated levels of urea, creatinine, citrate, glucose, glycerol, and phenylalanine and phenylalanine-to-tyrosine ratio (PTR) and (b) decreased levels of various amino acids (such leucine, isoleucine, valine, and alanine), high-density lipoproteins, lactate, and acetate. These changes suggested that CKD patients manifest severe oxidative

https://doi.org/10.1021/acsomega.2c06469
ACS Omega 2023, 8, 7722−7737

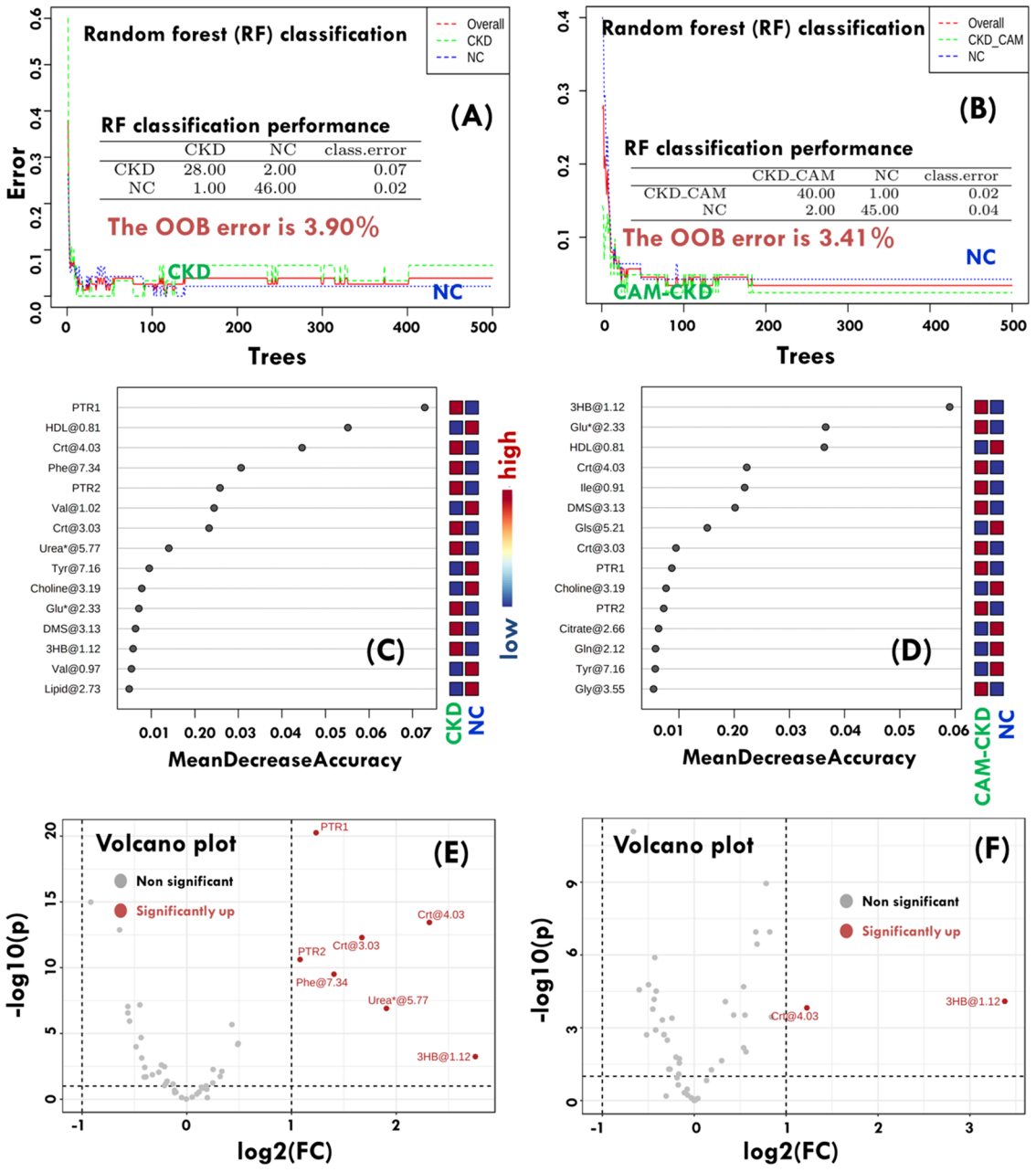

Figure 3. (A, B) Random forest (RF) classification models showing cumulative error rates measured for each class using the RF machine learning algorithm. The overall error rate is shown as the red line, and other color lines represent the error rates for each class as indicated. The out-of-bag (OOB) errors for each RF classification model are shown as insets. (C, D) Significant features were identified by ranking of mean decrease accuracy (MDA) extracted with RF analysis when the features are permuted. (E, F) Volcano plots reporting *p* values against fold changes. The volcano plot indicates −log 10 (*p* value) for serum metabolic profiles (*Y*-axis) plotted against their respective log 2 (fold change) (*X*-axis). Abbreviations used are as follows: Gls, glucose; Gln, glutamine; Glu, glutamate; PTR, phenylalanine-to-tyrosine ratio; His, histidine; PUFA, polyunsaturated fatty acid; Crt, creatinine; Cr, creatine; Ile, isoleucine; LDL, low-density lipoproteins; VLDL, very-low-density lipoproteins; HDL, high-density lipoproteins. As noted here, spectral bins with an asterisk "*" represent the cumulative signal of bins corresponding to the specified metabolite peak at that ppm. Bins specified by an even number for the last decimal place represent the cumulative signals of two adjacent bins, e.g., Leu@0.94 represents the sum of Leu@0.93 and Leu@0.95 and like this for other such features; PTR1 is evaluated as (Phe@7.30 + Phe@7.34)/Tyr@7.16, and PTR2 is evaluated as Phe@7.39/Tyr@6.87.

stress, hyperglycemia (with dampened glycolysis), and increased protein energy wasting.

Cross-Validation of Metabolic Changes in CKD and CAM-CKD Patients. To make a reliable comparison between clinical subtypes, a validation cohort of CAM-CKD patients (*N* = 26) was further included for which the clinical and demographic details are added in Table 1. Figure 5 compares the serum metabolic features of CKD patients with the second cohort of CAM-CKD patients (referred here to as CAM-CKD_2) having dominance of stage 5 patients (total of 10 in number). Both CKD and CAM-CKD_2 patients conferred almost similar patterns of metabolic disturbances as observed for the comparison of CKD with CAM-CKD patients, e.g., elevated phenylalanine and phenylalanine-to-tyrosine ratio (PTR, indicative of oxidative stress condition) both in CKD and CAM-CKD cases with respect to NC subjects. Compared to

https://doi.org/10.1021/acsomega.2c06469
ACS Omega 2023, 8, 7722−7737

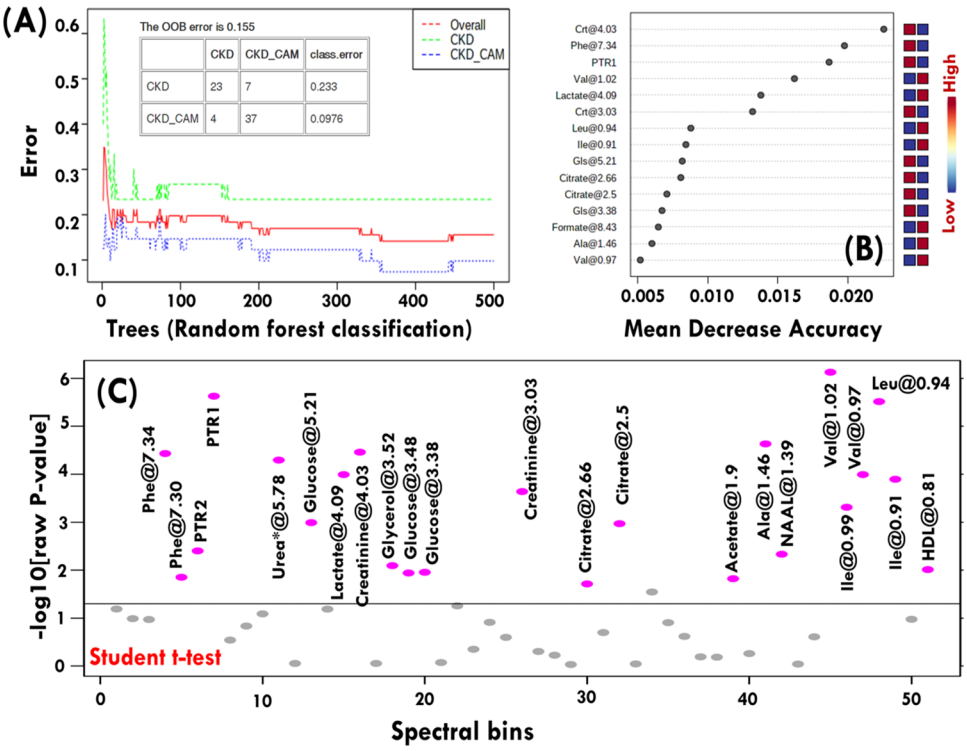

Figure 4. (A) Random forest (RF) classification model showing cumulative error rates measured for each class using the RF machine learning algorithm and the out-of-bag (OOB) error shown as an inset. The overall error rate is shown as the red line, and other color lines represent the error rates for each class as indicated. (B) Discriminatory features were identified by ranking of mean decrease accuracy (MDA) value based on RF analysis when the features are permuted and further evaluated for their statistical significance employing Student *t*-test plot shown in panel (C). Abbreviations used are as follows: Gls, glucose; Gln, glutamine; Glu, glutamate; PTR, phenylalanine-to-tyrosine ratio; His, histidine; PUFA, polyunsaturated fatty acid; Crt, creatinine; Cr, creatine; Ile, isoleucine; LDL, low-density lipoproteins; VLDL, very-low-density lipoproteins; HDL, high-density lipoproteins. As noted here, spectral bins with an asterisk "*" represent the cumulative signal of bins corresponding to the specified metabolite peak at that ppm. Bins specified by an even number for the last decimal place represent the cumulative signals of two adjacent bins, e.g., Leu@0.94 represents the sum of Leu@0.93 and Leu@0.95 and like this for other such features; PTR1 is evaluated as (Phe@7.30 + Phe@7.34)/Tyr@7.16, and PTR2 is evaluated as Phe@7.39/Tyr@6.87.

CAM-CKD_2, the degree of elevation of phenylalanine and PTR was relatively higher in CKD (Figure 5), the finding of which was in line with previous comparative analysis (Figure 4). Persistently, the serum creatinine, urea, and glucose levels were found to be significantly higher in CKD patients compared to CAM-CKD_2 patients with respect to NC subjects (Figure 5). Another important serum metabolic change observed was elevated serum levels of myoinositol and decreased serum levels of HDL (high-density lipoproteins) in CKD patients compared to CAM-CKD_2 patients with respect to NC subjects (Figure 5). The comparative analysis further validated our metabolic hallmark that the CKD patients exhibited more aberrant serum metabolic changes compared to the CAM-CKD_2 patient cohort with respect to NC subjects.

Further, we cross-validated the intervention effect of using CAM by CKD patients by comparing the serum metabolic profiles of stage 5 CKD patients (N = 17) with stage 5 CAM-CKD patients (N = 17, 7 from the first cohort and 10 from the second cohort). The results of PLS-DA-based multivariate analysis are summarized in Figure 5, and those based on OPLS-DA and RF classification analysis are included in the Supporting Information (see Figure S6). The OPLS-DA model constructed using three components (p1, o1, and o2) presents a good classification for discrimination between stage 5 CKD (N = 17) and CAM-CKD (N = 17) patients with R2X(cum) = 0.445, R2Y(cum) = 0.814, and Q2 = 0.552 (see the Supporting Information, Figure S6). Compared to CAM-CKD stage 5 patients, the serum levels of LDL/VLDL and creatinine were high in CKD stage 5 patients and those of various amino acids (such as branched chain amino acids, lysine, arginine, etc.; see the Supporting Information, Table S6) and of organic acids such as acetate were decreased in CKD stage 5 patients (Figure 6).

Next, the serum metabolic profiles of CAM-CKD stage 3 patients (N = 19, 12 from the first cohort and 7 from the second cohort) with stage 5 patients (N = 17, 7 from the first cohort and 10 from the second cohort). The results based on OPLS-DA and RF classification analysis are included in the Supporting Information (see Figure S7). The OPLS-DA model constructed using four components (p1, o1, o2, and o3) presents a good classification for discrimination between stage 3 CAM-CKD (N = 17) and stage 5 CAM-CKD (N = 17) patients with R2X(cum) = 0.625, R2Y(cum) = 0.729, and Q2 = 0.342 (see the Supporting Information, Figure S7). Compared to stage 3 CAM-CKD patients, the serum levels of lipid metabolites (including LDL/VLDL and PUFA) were decreased in stage 5 patients, whereas those of ketone bodies (such as 3-hydroxy butyrate) were increased in stage 5 patients (Figure 7B).

DISCUSSION

The aim of the present study was to characterize the serum metabolic disparity between CKD and CAM-CKD patients with respect to healthy normal control (NC) subjects and to suggest distinctive metabolic signatures of the disease that would be

https://doi.org/10.1021/acsomega.2c06469
ACS Omega 2023, 8, 7722−7737

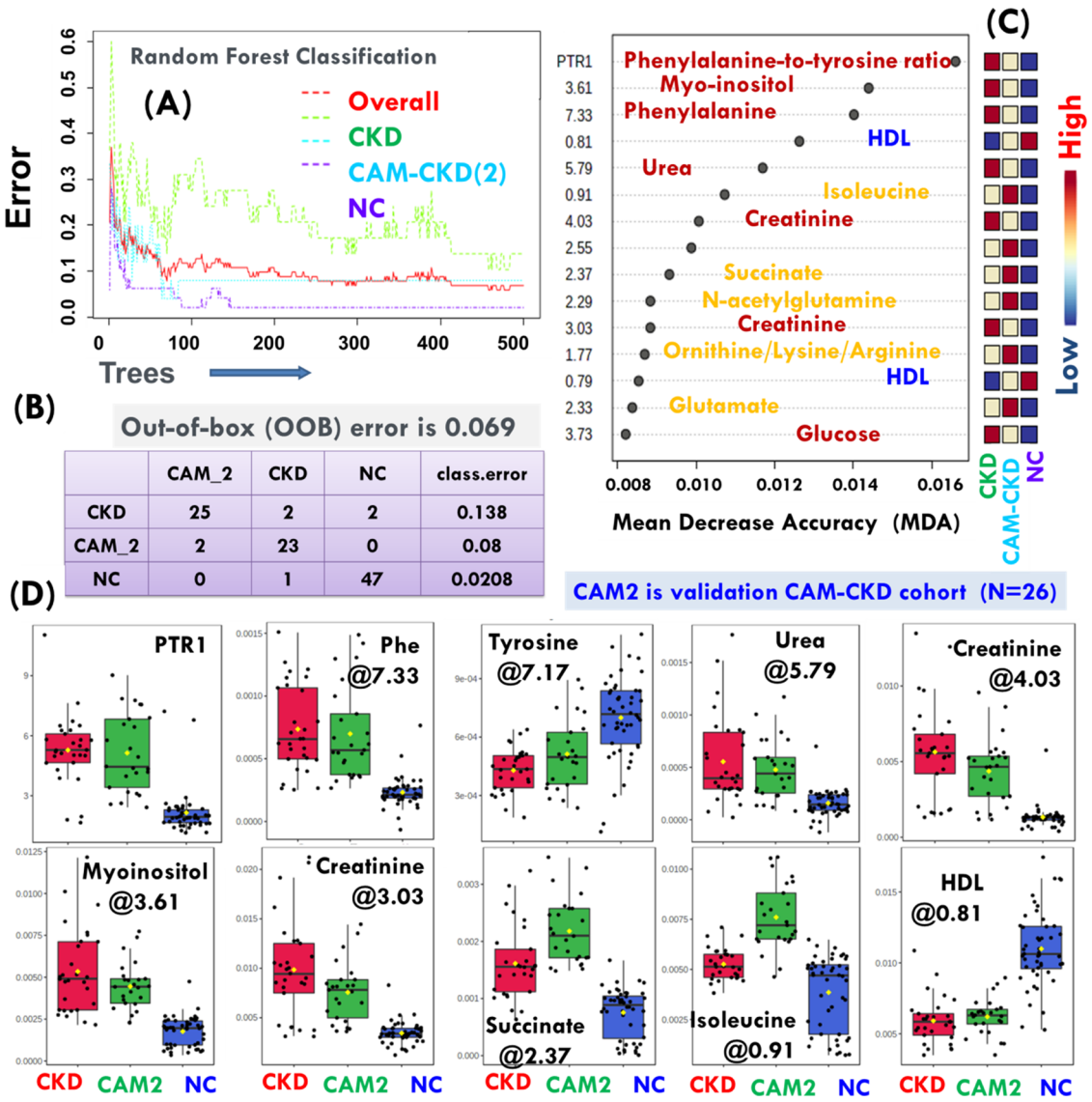

	CAM_2	CKD	NC	class.error
CKD	25	2	2	0.138
CAM_2	2	23	0	0.08
NC	0	1	47	0.0208

Figure 5. Serum metabolic profiles of CKD (N = 29, one identified as an outlier) patients and validation cohort of CAM-CKD (N = 26) patients (labeled here as CAM2) compared using the random forest (RF) classification method. (A) Random forest (RF) classification model showing cumulative error rates measured for each class using the RF machine learning algorithm. The overall error rate is shown as the red line, and other color lines represent the error rates for each class as indicated. (B) The out-of-bag (OOB) error for the RF model was found to be 6.9%, suggesting the high prediction accuracy of the RF model, that is, 93.1%. (C) Mean decrease accuracy (MDA) score plot highlighting the serum metabolic features of discriminatory potential. (D) Representative box-cum-whisker plots showing a metabolic change in CKD (red) and CAM2 (green) patients with respect to normal control subjects (in blue). For each box plot showing quantitative variations of relative NMR signal integrals, the boxes denote interquartile ranges, the horizontal red line inside the box denotes the median, and the bottom and top boundaries of the boxes are the 25th and 75th percentiles, respectively. Lower and upper whiskers are the 5th and 95th percentiles, respectively. Abbreviations used as follows: Phe, phenylalanine; PTR, phenylalanine-to-tyrosine ratio; HDL, high-density lipoprotein.

useful in guiding clinical treatment. The RF classification model clearly revealed that the metabolic changes are aberrantly different in CKD patients compared to CAM-CKD with respect to NC subjects. The metabolic changes exquisitely reflected the variability of biochemical processes underlying the pathophysiology of CKD. Consistent with biochemical features of CKD, the circulatory levels of creatinine were found to be significantly increased in CKD and CAM-CKD patients compared to NC subjects. Among patients, the serum levels of creatinine were found to be significantly increased in CKD compared to CAM-CKD (Figure 3).

Consistent with a previous report,[38] the circulatory levels of branched chain amino acids (such as valine,[39−41] leucine, and isoleucine) were found to be decreased in CKD patients compared to CAM-CKD patients with respect to NC subjects, suggesting a progressively increasing malnutritional status in CKD patients.

Compared to CAM-CKD patients, the circulatory urea levels were significantly higher in CKD patients with respect to NC (Figure 2D). Urea, a marker of uremic retention, has now been considered toxic at concentrations representative in CKD[42] and further increases insulin resistance and suppresses insulin secretion.[43,44] The finding is well in line with the elevated circulatory glucose levels in CKD patients compared to normal control and highlights the importance of management of hyperglycemia in CKD patients.[45] Studies have shown that the

https://doi.org/10.1021/acsomega.2c06469
ACS Omega 2023, 8, 7722−7737

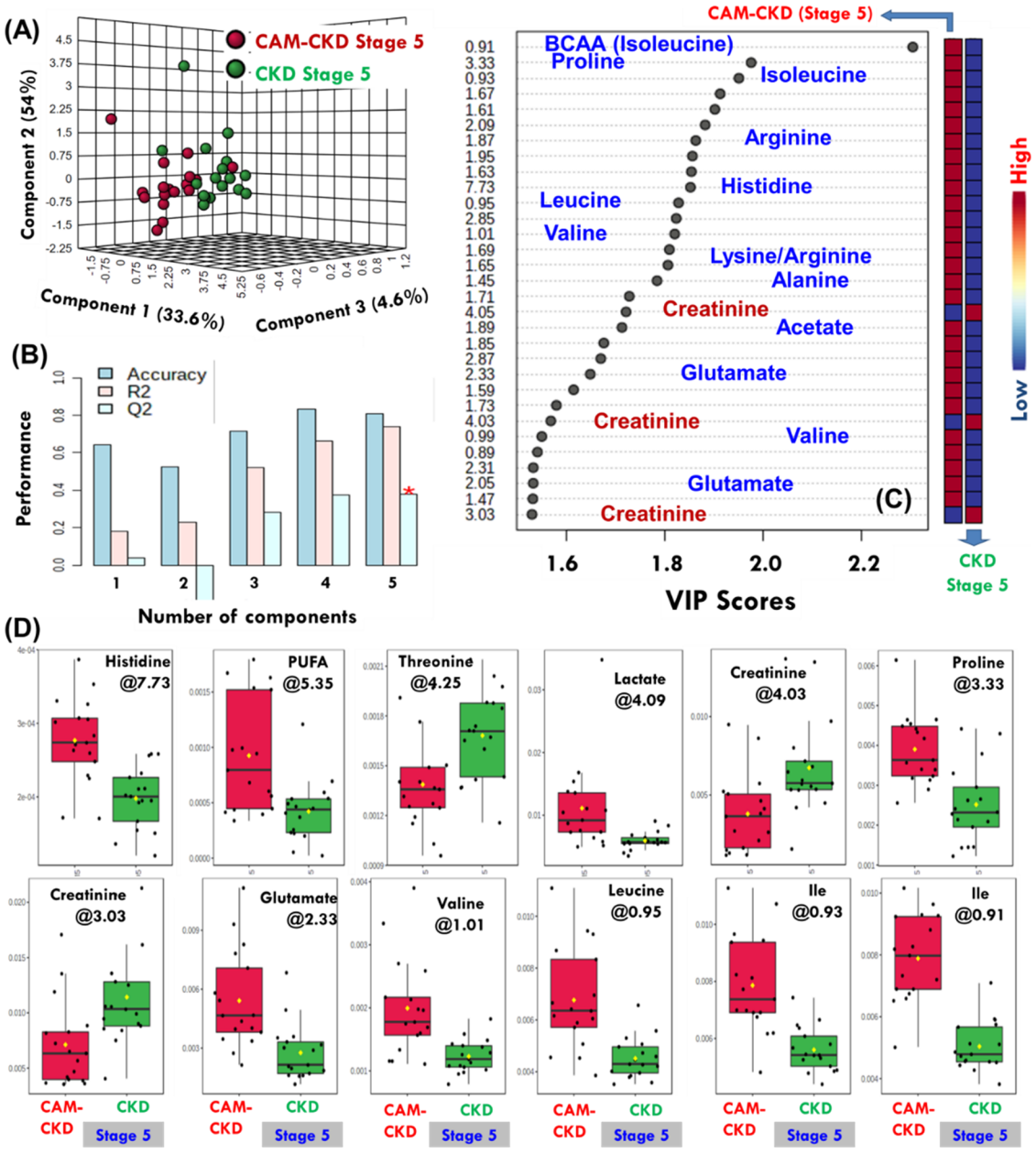

Figure 6. Serum metabolic profiles of stage 5 CKD ($N = 17$) and CAM-CKD ($N = 17$) patients compared using PLS-DA-based discriminatory analysis. (A) 3D PLS-DA score plot derived from the normalized spectral features and (B) performance of the PLS-DA classification model generated using different numbers of components. The red star indicates the best classifier. (C) Variables situated at the top right end are increased, while those situated at the lower left side are decreased in the sera of CKD patients compared to CAM-CKD patients. (D) Representative box-cum-whisker plots showing relative metabolic changes in stage 5 CKD patients (in green) compared to stage 5 CAM-CKD patients (in red). For each box plot showing quantitative variations of relative NMR signal integrals, the boxes denote interquartile ranges, the horizontal red line inside the box denotes the median, and the bottom and top boundaries of the boxes are the 25th and 75th percentiles, respectively. Lower and upper whiskers are the 5th and 95th percentiles, respectively. Abbreviations used as follows: PUFA, polyunsaturated fatty acids; Ile, isoleucine.

increased availability of urea also leads to elevated levels of cyanate and, hence, carbamylated compounds, which interfere with organ and body functions through multiple mechanisms.[42] Elevated circulatory levels of urea have been implicated in the development of oxidative stress and insulin resistance[46] in CKD, and nutritional management of urea levels has been demonstrated to slow the decline in renal function.[46] Compared to NC, the CKD patients manifested higher oxidative stress as inferred from the elevated circulatory levels of phenylalanine and phenylalanine-to-tyrosine ratio (PTR, which is known to serve as an indicative biomarker of oxidative stress in different pathophysiological conditions).[33−37] The statistically significant and positive correlation of circulatory PTR levels (Figure 4) with serum creatinine levels further suggested their association with the severity of the disease and may serve as a surrogate marker to improve the diagnostic/prognostic screening of CKD. Several studies have shown that oxidative stress (due to both antioxidant depletions and increased ROS production) disrupts mitochondrial homeostasis and, thus, normal functioning of kidney cells, which are metabolically highly active and rich in oxidation reactions in mitochondria.[47,48] Oxidative stress is among the leading mechanisms of cardiovascular complications,

https://doi.org/10.1021/acsomega.2c06469
ACS Omega 2023, 8, 7722−7737

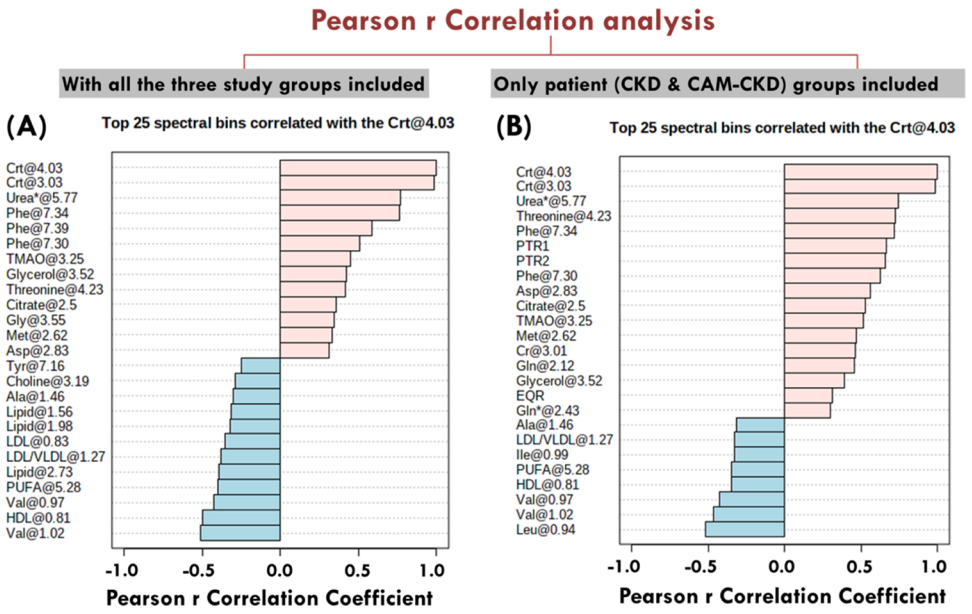

Figure 7. Serum metabolic features subjected to Pearson *r*-based correlation analysis with creatinine. The plots in panels (A) and (B) represent when the correlation analysis performed involves features (A) from all the three study groups and (B) from patient (i.e., CKD and CAM-CKD) groups. The explicit correlation values with their corresponding *p* values are tabulated in the Supporting Information (see Table S5A,B).

and in patients at advanced stages of CKD, increased oxidative stress is associated with profound dysregulation of lipid metabolism and marked abnormalities of serum lipid profiles.[49,50] Studies have shown that oxidative stress plays a key role in inducing dyslipidemia,[49,50] possibly through oxidation of lipoprotein/lipid metabolites in CKD, with this oxidation further increasing the risk of CVD.[51,52] Significantly higher cardiovascular morbidity and mortality in CKD patients have also been attributed to dyslipidemia.[53] This can be attributed to formation of atherosclerotic plaques as oxidized lipoproteins play a crucial role in atherosclerosis initiation and progression through chemotactic and proliferating actions on monocytes/macrophages, inciting their transformation into foam cells.[54−56] A recent NMR-based serum metabolomics study revealed decreased circulatory levels of lipid and membrane metabolites in CKD patients.[57] The NMR signals of lipoproteins have also been found to be decreased in the sera obtained from acute myocardial infarction (AMI) patients admitted to the intensive care unit (ICU).[58] Consistent with these metabolomics studies, the NMR signals of lipoproteins (including HDL, LDL, and VLDL) and lipid metabolites were found to be significantly decreased in CKD/CAM-CKD patients compared to NC. Contrary to this, the NMR signals of lipoproteins (LDL and VLDL) and lipid metabolites are significantly elevated in patients with lupus nephritis,[59,60] suggesting that CKD patients might share a CVD-like dyslipidemia pattern. Oxidative stress is often associated with inflammatory condition; however, the inflammatory state was not evident from the present metabolomics analysis and found to be consistent with previous clinical reports[38] and NMR-based serum metabolomics study.[15] The decreased NMR signals of *N*-acetyl glycoproteins (NAGs) in CKD patients could be attributed to the overlap of NAG signal with NMR signals of lipid metabolites, which are aberrantly decreased in these patients.

Consistent with various previous reports, the serum levels of myoinositol were found to be elevated in CKD patients (Figure 5B).[39−41] Compared to CAM-CKD patients, the serum levels of myoinositol in CKD patients increased apparently, further supporting the finding that the disease is more severe in CKD patients not using CAM (Figure 5B,D).

UNDERLYING RATIONALE FOR THE INTERVENTION EFFECT OF CAM IN CKD

Epidemiological studies have demonstrated that CKD patients show high cardiovascular morbidity and mortality and approximately 50% mortality of ESRD patients is due to cardiovascular disease (CVD).[61,62] The key factor inducing CVD in patients with kidney diseases is suggested to be oxidative stress[32,63,64] and its impact on dysregulation of lipid metabolism and abnormal serum lipid profiles.[49,50] The present study revealed that the circulatory levels of phenylalanine and PTR are significantly increased in CKD patients compared to CAM-CKD patients (w.r.t. NC subjects), suggesting that the use of CAM is conferring positive effects by ameliorating the systemic oxidative stress in CKD patients. The elevated oxidative stress has been suggested to play a key role in numerous clinical complications and adversely lead CKD patients' progression to end-stage renal disease (ESRD).[64] Based on literature reports and the findings of this study, we believe that effective management of oxidative stress in early stage CKD patients will serve to both slow the rate of progression of CKD to ESRD and reduce the risk of developing CVD complications. Indeed, several previous studies investigated anti-oxidant treatments in CKD patients and showed a reduction in oxidative stress and many showed improved renal function.[64] A PLS-DA analysis based on the pruned data matrix containing 51 spectral features (see the Supporting Information, Table S1) resulted in exquisite separation between the study groups, which was comparable to that obtained with the complete data matrix (see the Supporting Information, Figure S1).

CONCLUDING REMARKS

The study revealed serum metabolic differences between CKD patients with and without CAM. This observation may provide

https://doi.org/10.1021/acsomega.2c06469
ACS Omega 2023, 8, 7722−7737

an important clue to understanding the differences in the metabolic derangement between the two groups of CKD patients. Compared to the CAM-CKD group, the patients in the CKD group manifested higher oxidative stress as inferred from the elevated circulatory levels of phenylalanine and phenylalanine-to-tyrosine ratio. The statistically significant and positive correlation of circulatory PTR levels (Figure 7) with serum creatinine levels further suggested their association with the severity of the disease and may serve to improve the prognostic screening of CKD. Further, significantly decreased serum levels of branched chain amino acids (such as valine and leucine) in CKD patients ($p < 0.05$) were found to be well consistent with a previous report,[38] and their negative correlation with the serum creatinine level suggested a depressed nutritional status in these patients (Figure 7). However, these preliminary results require further validation to functionally associate oxidative stress with the severity of CKD. As mentioned here, the low circulatory PTR levels in the CAM-CKD group (but significantly higher compared to the NC group) can also be attributed to the less number of late stage CKD patients in this group. As the sample size of the present study is very small and, further, there is variability in the number of samples in different stages of CKD, we failed to perform the stage-wise comparison between CKD and CAM-CKD groups. Nevertheless, the study results were found to be well consistent with various previous reports,[41,65] especially the use of NMR-based serum levels of myoinositol, creatinine (both elevated and inversely correlated to GFR), and valine (decreased and positively correlated to GFR) for the estimation of GFR[41] in combination with the immunoturbidometric quantification of serum cystatin C, age, and sex.

Compared to the NC group, the observed metabolic changes in CKD patients were found to be in good concordance with various previous studies. Therefore, it is legitimate to believe that the disease-induced metabolic changes in CKD patients subdue those induced by different confounding factors such as BMI, diet, exercise, etc., when compared with respect to the normal control (NC) subject. However, the impact of confounding factors on the relative metabolic changes between CKD and CAM-CKD patients cannot be ignored. For example, studies have shown a strong geographic influence on the metabolome of CKD patients and further association between the body mass index (BMI) and risk for CKD.[66−68] Therefore, confounder-induced differences, such as BMI, diet, exercise, etc., may impact metabolic dysregulations in CKD patients and a careful evaluation of these factors on the metabolome of CKD patients needs to be considered in future studies.

As further mentioned here, the metabolic differences in our present study have been derived from normalized spectral features, which may provide ambiguous information when the corresponding bin contains signals from multiple metabolites. For example, the spectral bin at 3.23 ppm, which mainly represents glucose, does have contribution of NMR signals from GPC and trimethylamine-*N*-oxide (TMAO). Other than this, the subtle but significant metabolic changes may fail to show off in the VIP score plot or MDA plot in the presence of dominant signals of lipoproteins (LDL and VLDL), lipid/membrane metabolites, glucose, and lactate, which further contribute to multiple spectral bins as well. In summary, we demonstrated that serum metabolic profiles are aberrantly changed in CKD patients compared to CAM-CKD patients, and the use of CAM strongly affected the metabolic phenotypes of CKD patients and so the progression of disease to advanced stages of CKD. The findings of this study may also be used for guiding the future clinical and preclinical metabolomics studies related to evaluating the therapeutic efficacy and safety, especially, of CAM treatments.

MATERIALS AND METHODS

Recruitment of Subjects. The study protocol was approved by the institutional research and ethical committee, SGPGIMS, Lucknow, India (IEC code: 2015-92-EMP-EXP; file no. PGI/BE/607/2016; date of approval: 06 October 2016), and written informed consent was obtained from all of the patients before enrollment in the study. The blood samples from the peripheral vein were obtained (after overnight fasting) from 30 CKD and 43 CAM-CKD patients (between the years 2017 and 2018) and, for comparative evaluation, 47 age- and sex-matched normal healthy subjects (mostly kins or guardians of the patients). As the study involved the analysis of serum samples, therefore, serum tubes were used to collect the blood, incubated at ambient room temperature of 25 °C, and then the tube was centrifuged at 1200 rpm for 15 min at 4 °C. The supernatant (which represents the serum) was stored in 1.5 mL microcentrifuge (Eppendorf type) tubes and kept at −80 °C until the NMR analysis.

NMR Measurements and Spectral Data Processing. For NMR measurements, the samples were prepared following the procedure as described previously.[19,60] Briefly, the stored serum samples were thawed at room temperature and vortexed and 300 μL of serum was mixed with 300 μL of saline sodium phosphate buffer solution (buffer strength, 20 mM; 100% D_2O; containing 0.9% NaCl). After centrifugation (12,000 rpm, 10 min), 550 μL of supernatant was transferred to a 5 mm NMR tube. The samples were kept at 4 °C until measurement. The NMR spectra on all the serum samples were recorded at 300 k using an Avance III 800 MHz NMR spectrometer (Bruker, GmBH, Germany) equipped with Cryoprobe. The NMR spectra of the serum samples were recorded by using the transverse relaxation-edited 1D ^{1}H CPMG (Carr−Purcell−Meiboom−Gill) NMR spectra with water presaturation (employing the standard Bruker library pulse program cpmgpr1d). For each sample, 128 subsequent scans were collected with a spin-echo delay of 300 μs; there were 128 loops, a relaxation delay of 5 s, an acquisition time of 2.045 s, a time domain of 64 k, and a spectral width of 20.03 ppm. The recorded CPMG NMR spectra were processed using the standard Fourier transformation (FT) procedure in Bruker NMR data processing software named Topspin (v3.6, Bruker Biospin, Germany). Each FID was zero-filled to 64 k data points, and an exponential broadening of 3 Hz was applied prior to the Fourier transformation. All spectra were calibrated w.r.t. lactate-CH_3 signal at δ(1.31 ppm) following manual phase and baseline correction. The ^{1}H NMR peaks in highly overlapped and complex spectral regions of the 1D ^{1}H CPMG NMR spectra were identified and assigned, making composite use of the 2D JRES, homonuclear ^{1}H−^{1}H TOCSY (total correlation spectroscopy), and heteronuclear ^{1}H−^{13}C HSQC (heteronuclear single quantum correlation) spectra recorded on selected samples. For this, the information provided by the 1D CPMG spectra was combined with the 2D JRES, ^{1}H−^{1}H TOCSY, and ^{1}H−^{13}C HSQC NMR spectra and compared with the libraries of ^{1}H and ^{13}C chemical shifts reported in the literature for compounds commonly found in the serum in addition to those given in the freely available software MetaboMiner[69] following the procedural steps described previously.[70−72]

https://doi.org/10.1021/acsomega.2c06469
ACS Omega 2023, 8, 7722−7737

The present study involved the comparative analysis of normalized spectral features obtained by dividing each spectrum ranging from 0.6 to 8.6 ppm into equal sized bins of 0.02 and 0.01 ppm using Bruker AMIX software (version 3.8.7, Bruker GmbH, Germany). Depending upon the ppm span of the peak(s) of a particular metabolite, the bins were selected strategically either from 0.02 or 0.01 ppm binned data matrices (explicit information is evident from the legends of the different tables). The variability due to the residual water signal was removed by discarding the spectral region δ(4.5 to 5.1 ppm) prior to binning. The total intensity sum of the spectral bins was used to normalize the integral value of each spectral bin. The resulted data matrix containing normalized spectral bins (or features) was then subjected to multivariate and univariate statistical analyses. Two metabolic features (PTR1 and PTR2) representing the phenylalanine-to-tyrosine ratio (PTR) were additionally included in the data matrix and evaluated as follows: PTR1 = (Phe@7.30 + Phe@7.34)/Tyr@7.16 and PTR2 = Phe@7.39/Tyr@6.87. The spectral bins were annotated manually with the help of NMR Suite of commercial software Chenomx v8.6 (Edmonton, Alberta, Canada), which has the advantage of a database of standard metabolite spectra at a variety of magnetic field strengths and a variety of pH values.[73]

Multivariate Analysis. Multivariate analysis (MVA) is used to transform the complex multivariate data into easily understandable graphical representations and identify discriminatory variables. MVA was performed using statistical analysis modules of MetaboAnalyst (v5.0, a freely available, user-friendly, web-based analytical platform for metabolomics data analysis from the University of Alberta, Canada: www.metaboanalyst.ca).[74−76] The analysis was performed following the procedure as described previously.[77,78] Briefly, the CPMG data matrix containing normalized spectral bins was pareto-scaled (mean-centered and divided by the square root of the standard deviation of each variable) and subsequently subjected to unsupervised principal component analysis (PCA) for an initial overview of the grouping trend (i.e., intrinsic clustering) and outliers within the data set. After initial overview and identification of the outliers, the supervised clustering method, i.e., partial least-squares discriminant analysis (PLS-DA), was used as a diagnostic model to identify the distinguishing features and further to identify the marker metabolites that can differentiate the CKD and CAM-CKD patient groups from the normal control (NC) group. Compared to PCA, PLS-DA inclines to overfit the data and so maximizes the class discrimination. Therefore, PLS-DA models were rigorously validated by the default 10-fold cross-validation algorithm, which helps to evaluate 100% classification accuracy using the top 5 latent variables.[76] The quality of the models was assessed by R^2 (goodness of fit parameter) and Q^2 (predictive ability parameter) values. As such, R^2 represents the proportion of variance in the data explained by the models and Q^2 represents the proportion of variance in the data predicted by the model.[78,79] The performance of PLS-DA models was further improved by OPLS-DA. OPLS-DA is an extension of PLS-DA featuring an integrated orthogonal signal correction (OSC) filter to remove variability not relevant to class separation.[19,80] The metabolites of discriminatory potential were identified from the PLS-DA model based on their higher ranking in the VIP (variable importance on projection) score plot.[81] The supervised random forest (RF) classification analysis was performed within the statistical analysis module of MetaboAnalyst.[82,83] The discriminatory variables/features are ranked in RF by their contributions to classification accuracy, i.e., mean decrease accuracy (MDA) quantifies the discriminatory importance of a variable by measuring the change in prediction accuracy when the values of the variable are randomly permuted compared to the original observations.[84−86] As mentioned here, the MDA-based feature selection method does consider the statistical classification without any biological significance.[85,87] The metabolic features with MDA $\geq$ 0.01 were considered as of discriminatory potential and further subjected to univariate statistical testing using variants of *t*-test: (a) Mann−Whitney *U* test to compare continuous data between two groups and (b) volcano plot and one-way analysis of variance (ANOVA) for comparison between three groups. This analysis was used to evaluate the statistical significance and performed using the "Statistical analysis" module of MetaboAnalyst,[75,76] and the level of statistical significance was set at $p < 0.05$. The results are summarized in the Supporting Information (Tables S2−S4 for normal control subjects and patient samples). The standard box plot representations were used to visualize the variation in the levels of significantly altered metabolites. The key metabolic changes were further evaluated for diagnostic potential using receiver operating characteristic (ROC) curve analysis performed with the "Biomarker analysis" module of MetaboAnalyst,[75,76] and the area under the ROC (AUROC) curve of more than 0.9 was considered the criterion for diagnostic performance. Continuous variables were expressed as the mean ± SD and categorical variables as the percentage.

Correlation Analysis. Circulatory creatinine levels were regressed against other metabolic levels to identify metabolites that correlated with serum creatinine levels. The results are summarized in the Supporting Information (Table S5A,B for normal control subjects and patient samples).

■ ASSOCIATED CONTENT

Supporting Information

The Supporting Information is available free of charge at https://pubs.acs.org/doi/10.1021/acsomega.2c06469.

Table S1: 51 spectral bins of 0.02 ppm selected from the CPMG data matrix for multivariate statistical analysis; Table S2: serum metabolic entities exhibiting statistically significant difference between the study groups evaluated using ANOVA statistics based on Fisher's least significant difference (LSD, a commonly used post hoc test); Table S3: important spectral features identified by the volcano plot; Table S4: serum metabolic entities exhibiting statistically significant difference between the study groups evaluated using ANOVA statistics based on Fisher's least significant difference (LSD, a commonly used post hoc test); Table S5: Pearson *r* correlation of creatinine (selecting spectral bin @4.03 ppm) with other NMR-based serum metabolic features; Table S6: top 50 normalized spectral features exhibiting statistically significant difference between stage 5 CKD and CAM-CKD patients identified by *t*-tests; Figure S1: graph plot showing the number of serum samples collected in each clinical subtype of CKD patient; Figure S2: stack plot of cumulative 1D ^{1}H CPMG NMR spectra of CKD and CAM-CKD patients showing the metabolite assignment of NMR peaks and using various NMR methods; Figure S3: PLS-DA-based multivariate statistical analysis performed using normalized spectral features obtained for serum samples of CKD (red) and CAM-CKD (green)

https://doi.org/10.1021/acsomega.2c06469
ACS Omega 2023, 8, 7722−7737

patients and normal control subjects (in blue) and further identification of metabolic features of discriminatory potential; Figure S4: box-cum-whisker plots showing relatively metabolic changes between CKD (red) and CAM-CKD (green) patients with respect to normal control (NC, in blue) subjects; Figure S5: box-cum-whisker plots showing statistically significant metabolic change between CKD (red) and CAM-CKD (green) patients; Figure S6: multivariate analysis comparing serum metabolic profiles of stage 5 CKD (N = 17) and CAM-CKD (N = 17) patients using OPLS-DA and random forest (RF) classification methods; Figure S7: multivariate analysis comparing serum metabolic profiles of stage 3 (N = 19) and stage 5 (N = 17) CAM-CKD patients using OPLS-DA and random forest (RF) classification methods (PDF)

AUTHOR INFORMATION

Corresponding Authors

Dinesh Kumar − *Centre of Biomedical Research (CBMR), Lucknow, Uttar Pradesh 226014, India*; Email: dineshcbmr@gmail.com, dinesh@cbmr.res.in

Narayan Prasad − *Department of Nephrology, SGPGIMS, Lucknow, Uttar Pradesh 226014, India*; Email: narayan.nephro@gmail.com

Authors

Nikhil Gupta − *Centre of Biomedical Research (CBMR), Lucknow, Uttar Pradesh 226014, India; Department of Chemistry, Banaras Hindu University, Varanasi, Uttar Pradesh 221005, India*; orcid.org/0000-0002-9818-2206

Deependra Kumar Yadav − *Department of Nephrology, SGPGIMS, Lucknow, Uttar Pradesh 226014, India*

Sonam Gautam − *Department of Nephrology, SGPGIMS, Lucknow, Uttar Pradesh 226014, India*

Ashish Kumar − *Department of Chemistry, Banaras Hindu University, Varanasi, Uttar Pradesh 221005, India*

Complete contact information is available at: https://pubs.acs.org/10.1021/acsomega.2c06469

Author Contributions

‖N.G. and D.K.Y. contributed equally to this work.

Author Contributions

D.K.Y., S.G., and N.P. were involved in clinical evaluation, collecting patient samples, and compiling clinical details. N.G. and A.K. carried out the preparation of serum samples for NMR studies, NMR data collection, data processing, and manuscript drafting. D.K. conducted the metabolomics data analysis and manuscript preparation.

Notes

The authors declare no competing financial interest.

ACKNOWLEDGMENTS

D.K. acknowledges the Department of Science and Technology for financial assistance under SERB EMR Scheme (ref. no.: EMR/2016/001756) and the Department of Medical Education, Govt. of Uttar Pradesh, for supporting the High Field NMR Facility at the Centre of Biomedical Research, Lucknow, India. N.G. acknowledges receipt of the irregular SRF fellowship from CSIR, India (file number: 09/916(0096)/2018-EMR-I). This study was funded by Department of Biotechnology (DBT), Ministry of Science and Technology grant (Grant No. BT/PR11105/MED/30/1345/2014) under the project entitled "Indian Chronic Kideny Diseases study: Second Phase".

ABBREVIATIONS USED

CKD	chronic kidney disease
CAM	complementary and alternative medicines
CAM-CKD	CKD patients using CAM
ESRD	end-stage renal disease
DM	diabetes mellitus
T2DM	type II diabetic mellitus
ICU	intensive care unit
NC	normal control
NMR	nuclear magnetic resonance
CPMG	Carr−Purcell−Meiboom−Gill
PCA	principal component analysis
PLS-DA	partial least-square discriminant analysis
OPLS-DA	orthogonal signal-corrected PLS-DA
ROC	receiver operating characteristic
AUROC	area under the ROC curve
PUFA	polyunsaturated fatty acid
3HB	3-hydroxybutyrate
CI	confidence interval
SEM	standard error in mean
GFR	glomerular filtration rate
TMAO	trimethylamine-*N*-oxide
RF	random forest
OOB	out of bag
MDA	mean decrease accuracy
1D/2D	one/two dimensional
Crt	creatinine
NAAL	*N*-alpha acetyl lysine
TMA	trimethylamine
HDL	high-density lipoproteins
LDL	low-density lipoproteins
VLDL	very-low-density lipoproteins
GPC	glycerophosphocholine
DMS	dimethyl-sulfone
BCAA	branched-chain amino acid
Glu	glutamate
Gls	glucose
Gln	glutamine
NAG	*N*-acetyl glycoprotein
Tyr	tyrosine
Phe	phenylalanine
PTR	phenylalanine-to-tyrosine ratio

REFERENCES

(1) Levey, A. S.; Atkins, R.; Coresh, J.; Cohen, E. P.; Collins, A. J.; Eckardt, K. U.; Nahas, M. E.; Jaber, B. L.; Jadoul, M.; Levin, A.; Powe, N. R.; Rossert, J.; Wheeler, D. C.; Lameire, N.; Eknoyan, G. Chronic kidney disease as a global public health problem: approaches and initiatives-a position statement from Kidney Disease Improving Global Outcomes. *Kidney Int.* **2007**, *72*, 247−259.

(2) Saeed, S.; Islahudin, F.; Makmor-Bakry, M.; Redzuan, A. M. The practice of complementary and alternative medicine among chronic Kidney disease patients. *J. Adv. Pharm. Educ. Res.* **2018**, *8*, 31.

(3) Jha, V.; Garcia-Garcia, G.; Iseki, K.; Li, Z.; Naicker, S.; Plattner, B.; Saran, R.; Wang, A. Y.-M.; Yang, C. W. Chronic kidney disease: global dimension and perspectives. *Lancet* **2013**, *382*, 260−272.

(4) Davies, R. The metabolomic quest for a biomarker in chronic kidney disease. *Clin. Kidney J.* **2018**, *11*, 694−703.

(5) World Health Organization *WHO traditional medicine strategy: 2014−2023*. 2013,

(6) Hasan, S. S.; Ahmed, S. I.; Bukhari, N. I.; Loon, W. C. W. Use of complementary and alternative medicine among patients with chronic diseases at outpatient clinics. *Complement Ther. Clin. Pract.* **2009**, *15*, 152−157.
(7) Castelino, L. R.; Nayak-Rao, S.; Shenoy, M. P. Prevalence of use of complementary and alternative medicine in chronic kidney disease: a cross-sectional single-center study from South India. *Saudi J. Kidney Dis. Transpl.* **2019**, *30*, 185.
(8) Saydah, S. H.; Eberhardt, M. S. Use of complementary and alternative medicine among adults with chronic diseases: United States 2002. *J. Altern. Complementary Med.* **2006**, *12*, 805−812.
(9) Rao, A. S. A.; Phaneendra, D.; Pavani, C. D.; Soundararajan, P.; Rani, N. V.; Thennarasu, P.; Kannan, G. Usage of complementary and alternative medicine among patients with chronic kidney disease on maintenance hemodialysis. *J. Pharm. BioAllied Sci.* **2016**, *8*, 52.
(10) Prichard, S. S. Comorbidities and their impact on outcome in patients with end-stage renal disease. *Kidney Int.* **2000**, *57*, S100−S104.
(11) Hocher, B.; Adamski, J. Metabolomics for clinical use and research in chronic kidney disease. *Nat. Rev. Nephrol.* **2017**, *13*, 269−284.
(12) Kim, J. A.; Choi, H. J.; Kwon, Y. K.; Kwon, T. H.; Hwang, G. S. 1 H NMR-Based Metabolite Profiling of Plasma in a Rat Model of Chronic Kidney Disease. *PLoS One* **2014**, *9*, No. e85445.
(13) James, L. P. Metabolomics: integration of a new "omics" with clinical pharmacology. *Clin. Pharmacol. Ther.* **2013**, *94*, 547−551.
(14) Wu, I. W.; Gao, S. S.; Chou, H. C.; Yang, H. Y.; Chang, L. C.; Kuo, Y. L.; Dinh, M. C. V.; Chung, W. H.; Yang, C. W.; Lai, H. C.; Hsieh, W. P.; Su, S. C. Integrative metagenomic and metabolomic analyses reveal severity-specific signatures of gut microbiota in chronic kidney disease. *Theranostics* **2020**, *10*, 5398.
(15) Lee, J.; Choi, J. Y.; Kwon, Y. K.; Lee, D.; Jung, H. Y.; Ryu, H. M.; Cho, J. H.; Kim, Y. L.; Hwang, G. S. Changes in serum metabolites with the stage of chronic kidney disease: Comparison of diabetes and non-diabetes. *Clin. Chim. Acta* **2016**, *459*, 123−131.
(16) Hallan, S.; Afkarian, M.; Zelnick, L. R.; Kestenbaum, B.; Sharma, S.; Saito, R.; Darshi, M.; Barding, G.; Raftery, D.; Ju, W.; Kretzler, M.; Sharma, K.; de Boer, I. H. Metabolomics and gene expression analysis reveal down-regulation of the citric acid (TCA) cycle in non-diabetic CKD patients. *EBioMedicine* **2017**, *26*, 68−77.
(17) Missailidis, C.; Hällqvist, J.; Qureshi, A. R.; Barany, P.; Heimbürger, O.; Lindholm, B.; Stenvinkel, P.; Bergman, P. Serum trimethylamine-N-oxide is strongly related to renal function and predicts outcome in chronic kidney disease. *PLoS One* **2016**, *11*, No. e0141738.
(18) Hunter, E.; Percival, B.; Ahmad, Z.; Chang, M. W.; Hunt, J. A.; Tasker, S.; De Risio, L.; Wilson, P. B. NMR-based metabolomics associated with chronic kidney disease in humans and animals: a one health perspective. *Mol. Cell. Biochem.* **2021**, *476*, 4133−4137.
(19) Guleria, A.; Kumar, A.; Kumar, U.; Raj, R.; Kumar, D. NMR Based Metabolomics: An Exquisite and Facile Method for Evaluating Therapeutic Efficacy and Screening Drug Toxicity. *Curr. Top. Med. Chem.* **2018**, *18*, 1827−1849.
(20) Mula-Abed, W. A.; Al Rasadi, K.; Al-Riyami, D. Estimated glomerular filtration rate (eGFR): A serum creatinine-based test for the detection of chronic kidney disease and its impact on clinical practice. *Oman Med. J.* **2012**, *27*, 108.
(21) Ma, Y. C.; Zuo, L.; Chen, J. H.; Luo, Q.; Yu, X. Q.; Li, Y.; Xu, J. S.; Huang, S. M.; Wang, L. N.; Huang, W.; Wang, M.; Xu, G. B.; Wang, H. Y. Modified glomerular filtration rate estimating equation for Chinese patients with chronic kidney disease. *J. Am. Soc. Nephrol.* **2006**, *17*, 2937−2944.
(22) Levey, A. S.; Stevens, L. A.; Schmid, C. H.; Zhang, Y.; Castro, A. F., III; Feldman, H. I.; Kusek, J. W.; Eggers, P.; Van Lente, F.; Greene, T. A new equation to estimate glomerular filtration rate. *Ann. Intern. Med.* **2009**, *150*, 604−612.
(23) Levey, A. S.; Stevens, L. A.; Coresh, J. Conceptual model of CKD: applications and implications. *Am. J. Kidney Dis.* **2009**, *53*, S4−S16.
(24) Grissa, D.; Petera, M.; Brandolini, M.; Napoli, A.; Comte, B.; Pujos-Guillot, E. Feature selection methods for early predictive biomarker discovery using untargeted metabolomic data. *Front. Mol. Biosci.* **2016**, *3*, 30.
(25) Chen, T.; Cao, Y.; Zhang, Y.; Liu, J.; Bao, Y.; Wang, C.; Jia, W.; Zhao, A. Random forest in clinical metabolomics for phenotypic discrimination and biomarker selection. *J. Evidence-Based Integr. Med.* **2013**, *2013*, 298183.
(26) Modaresi, A.; Nafar, M.; Sahraei, Z. Oxidative stress in chronic kidney disease. *Iran. J. kidney dis.* **2015**, *9*, 165.
(27) Xu, G.; Luo, K.; Liu, H.; Huang, T.; Fang, X.; Tu, W. The progress of inflammation and oxidative stress in patients with chronic kidney disease. *Renal failure* **2015**, *37*, 45−49.
(28) Tucker, P. S.; Scanlan, A. T.; Dalbo, V. J. Chronic kidney disease influences multiple systems: describing the relationship between oxidative stress, inflammation, kidney damage, and concomitant disease. *Oxid. Med. Cell. Longevity* **2015**, *2015*, 1.
(29) Putri, A. Y.; Thaha, M. Role of oxidative stress on chronic kidney disease progression. *Acta Medica Indonesiana* **2014**, *46*, 244−252.
(30) Duni, A.; Liakopoulos, V.; Roumeliotis, S.; Peschos, D.; Dounousi, E. Oxidative stress in the pathogenesis and evolution of chronic kidney disease: untangling Ariadne's thread. *Int. J. Mol. Sci.* **2019**, *20*, 3711.
(31) Tirichen, H.; Yaigoub, H.; Xu, W.; Wu, C.; Li, R.; Li, Y. Mitochondrial reactive oxygen species and their contribution in chronic kidney disease progression through oxidative stress. *Front. Physiol.* **2021**, *12*, 398.
(32) Ravarotto, V.; Simioni, F.; Pagnin, E.; Davis, P. A.; Calo, L. A. Oxidative stress-chronic kidney disease-cardiovascular disease: a vicious circle. *Life Sci.* **2018**, *210*, 125−131.
(33) Fuchs, J. E.; Huber, R. G.; Von Grafenstein, S.; Wallnoefer, H. G.; Spitzer, G. M.; Fuchs, D.; Liedl, K. R. Dynamic regulation of phenylalanine hydroxylase by simulated redox manipulation. *PLoS One* **2012**, *7*, No. e53005.
(34) Geisler, S.; Gostner, J. M.; Becker, K.; Ueberall, F.; Fuchs, D. Immune activation and inflammation increase the plasma phenylalanine-to-tyrosine ratio. *Pteridines* **2013**, *24*, 27−31.
(35) Muhammed, H.; Kumar, D.; Dubey, D.; Kumar, S.; Chaurasia, S.; Guleria, A.; Majumder, S.; Singh, R.; Agarwal, V.; Misra, R. Metabolomics analysis revealed significantly higher synovial Phe/Tyr ratio in reactive arthritis and undifferentiated spondyloarthropathy. *Rheumatology* **2020**, *59*, 1587−1590.
(36) Murr, C.; Grammer, T. B.; Meinitzer, A.; Kleber, M. E.; Mñrz, W.; Fuchs, D. Immune activation and inflammation in patients with cardiovascular disease are associated with higher phenylalanine to tyrosine ratios: the ludwigshafen risk and cardiovascular health study. *J. amino acids* **2014**, 2014.
(37) Zangerle, R.; Kurz, K.; Neurauter, G.; Kitchen, M.; Sarcletti, M.; Fuchs, D. Increased blood phenylalanine to tyrosine ratio in HIV-1 infection and correction following effective antiretroviral therapy. *Brain Behav. Immun.* **2010**, *24*, 403−408.
(38) Kumar, M. A.; Bitla, A. R. R.; Raju, K. V. N.; Manohar, S. M.; Kumar, V. S.; Narasimha, S. R. P. V. L. Branched chain amino acid profile in early chronic kidney disease. *Saudi J. kidney Dis. Transplant* **2012**, *23*, 1202.
(39) Meeusen, J.; Stömmler, F.; Lieske, J.; Grassi, M.; Shah, M.; Schiffer, E. Estimated GFR by Serum Myo-inositol, Valine, Creatinine, and Cystatin-c Outperforms Current CKD-epi Equations in Renal Transplant Recipients. *Am. J. Transplant.* **2021**, *21*, 587−588.
(40) Ehrich, J.; Dubourg, L.; Hansson, S.; Pape, L.; Steinle, T.; Fruth, J.; Höckner, S.; Schiffer, E. Serum Myo-Inositol, Dimethyl Sulfone, and Valine in Combination with Creatinine Allow Accurate Assessment of Renal Insufficiency-A Proof of Concept. *Diagnostics* **2021**, *11*, 234.
(41) Stämmler, F.; Grassi, M.; Meeusen, J. W.; Lieske, J. C.; Dasari, S.; Dubourg, L.; Lemoine, S.; Ehrich, J.; Schiffer, E. Estimating Glomerular Filtration Rate from Serum Myo-Inositol, Valine, Creatinine and Cystatin C. *Diagnostics* **2021**, *11*, 2291.
(42) Vanholder, R.; Gryp, T.; Glorieux, G. Urea and chronic kidney disease: the comeback of the century?(in uraemia research). *Nephrol., Dial., Transplant.* **2018**, *33*, 4−12.

https://doi.org/10.1021/acsomega.2c06469
ACS Omega 2023, 8, 7722−7737

(43) Xie, Y.; Bowe, B.; Li, T.; Xian, H.; Yan, Y.; Al-Aly, Z. Higher blood urea nitrogen is associated with increased risk of incident diabetes mellitus. *Kidney Int.* **2018**, *93*, 741−752.
(44) Kamal, A. Estimation of blood urea (BUN) and serum creatinine level in patients of renal disorder. *Indian J. Fundam. Appl. Life Sci.* **2014**, *4*, 199−202.
(45) Neto, P. A.; Gomes, H. V.; Campos, M. Management of hyperglycemia in patients with chronic kidney disease. *J. Nephrol.* **2013**, *26*, 629−635.
(46) Chauveau, P.; Aparicio, M. Benefits in nutritional interventions in patients with CKD stage 3-4. *J. Renal Nutr.* **2011**, *21*, 20−22.
(47) Daenen, K.; Andries, A.; Mekahli, D.; Van Schepdael, A.; Jouret, F.; Bammens, B. Oxidative stress in chronic kidney disease. *Pediatr. Nephrol.* **2019**, *34*, 975−991.
(48) Randa-Rivera, A. K.; Cruz-Gregorio, A.; Paricio-Trejo, O. E.; Pedraza-Chaverri, J. Mitochondrial redox signaling and oxidative stress in kidney diseases. *Biomolecules* **2021**, *11*, 1144.
(49) Vaziri, N. D.; Navab, M.; Fogelman, A. M. HDL metabolism and activity in chronic kidney disease. *Nat. Rev. Nephrol.* **2010**, *6*, 287−296.
(50) Vaziri, N. D.; Moradi, H. Mechanisms of dyslipidemia of chronic renal failure. *Hemodialysis Int.* **2006**, *10*, 1−7.
(51) Trpkovic, A.; Resanovic, I.; Stanimirovic, J.; Radak, D.; Mousa, S. A.; Cenic-Milosevic, D.; Jevremovic, D.; Isenovic, E. R. Oxidized low-density lipoprotein as a biomarker of cardiovascular diseases. *Crit. Rev. Clin. Lab. Sci.* **2015**, *52*, 70−85.
(52) Zhong, S.; Li, L.; Shen, X.; Li, Q.; Xu, W.; Wang, X.; Tao, Y.; Yin, H. An update on lipid oxidation and inflammation in cardiovascular diseases. *Free Radicals Biol. Med.* **2019**, *144*, 266−278.
(53) Bermudez-Lopez, M.; Arroyo, D.; Betriu, Á.; Masana, L.; Fernández, E.; Valdivielso, J. M. New perspectives on CKD-induced dyslipidemia. *Expert Opin. Ther. Targets* **2017**, *21*, 967−976.
(54) Holvoet, P.; Collen, D. Oxidized lipoproteins in atherosclerosis and thrombosis. *FASEB J.* **1994**, *8*, 1279−1284.
(55) Leeuwenburgh, C.; Rasmussen, J. E.; Hsu, F. F.; Mueller, D. M.; Pennathur, S.; Heinecke, J. W. Mass spectrometric quantification of markers for protein oxidation by tyrosyl radical, copper, and hydroxyl radical in low density lipoprotein isolated from human atherosclerotic plaques. *J. Biol. Chem.* **1997**, *272*, 3520−3526.
(56) Tsimikas, S.; Miller, I. Oxidative modification of lipoproteins: mechanisms, role in inflammation and potential clinical applications in cardiovascular disease. *Curr. Pharm. Des.* **2011**, *17*, 27−37.
(57) Qi, S.; Ouyang, X.; Wang, L.; Peng, W.; Wen, J.; Dai, Y. A pilot metabolic profiling study in serum of patients with chronic kidney disease based on 1H-NMR-Spectroscopy. *Clin. Transl. Sci.* **2012**, *5*, 379−385.
(58) Rawat, A.; Srivastava, R. K.; Dubey, D.; Guleria, A.; Singh, S.; Prakash, A.; Modi, D. R.; Khetrapal, C. L.; Tiwari, S.; Kumar, D. Serum metabolic disturbances hailing in initial hours of acute myocardial infarction elucidated by NMR based metabolomics. *Curr. Metabolomics* **2017**, *5*, 55−67.
(59) Guleria, A.; Phatak, S.; Dubey, D.; Kumar, S.; Zanwar, A.; Chaurasia, S.; Kumar, U.; Gupta, R.; Aggarwal, A.; Kumar, D.; Misra, R. NMR-Based Serum Metabolomics Reveals Reprogramming of Lipid Dysregulation Following Cyclophosphamide-Based Induction Therapy in Lupus Nephritis. *J. Proteome Res.* **2018**, *17*, 2440−2448.
(60) Guleria, A.; Pratap, A.; Dubey, D.; Rawat, A.; Chaurasia, S.; Sukesh, E.; Phatak, S.; Ajmani, S.; Kumar, U.; Khetrapal, C. L. NMR based serum metabolomics reveals a distinctive signature in patients with Lupus Nephritis. *Sci. Rep.* **2016**, *6*, 35309.
(61) Ikizler, T. A. Epidemiology of vascular disease in renal failure. *Blood Purif.* **2002**, *20*, 6−10.
(62) Kao, M. P. C.; Ang, D. S. C.; Pall, A. A.; Struthers, A. D. Oxidative stress in renal dysfunction: mechanisms, clinical sequelae and therapeutic options. *J. Hum. Hypertens.* **2010**, *24*, 1−8.
(63) Ling, X. C.; Kuo, K. L. Oxidative stress in chronic kidney disease. *Renal Replacement Therapy* **2018**, *4*, 53.
(64) Oberg, B. P.; McMenamin, E.; Lucas, F. L. E. E.; McMonagle, E.; Morrow, J.; Ikizler, T. A. L. P.; Himmelfarb, J. Increased prevalence of oxidant stress and inflammation in patients with moderate to severe chronic kidney disease. *Kidney Int.* **2004**, *65*, 1009−1016.
(65) Fuhrmann, M.; Schwaeble Santamaria, A.; Scott, R.; Meeusen, J. W.; Fernandes, M.; Venz, J.; Rothe, V.; Stämmler, F.; Ehrich, J.; Schiffer, E. Analytical Validation of GFRNMR: A Blood-Based Multiple Biomarker Assay for Accurate Estimation of Glomerular Filtration Rate. *Diagnostics* **2022**, *12*, 1120.
(66) Kalantari, S.; Nafar, M. An update of urine and blood metabolomics in chronic kidney disease. *Biomarkers Med.* **2019**, *13*, 577−596.
(67) Yamaguchi, Y.; Zampino, M.; Moaddel, R.; Chen, T. K.; Tian, Q.; Ferrucci, L.; Semba, R. D. Plasma metabolites associated with chronic kidney disease and renal function in adults from the Baltimore Longitudinal Study of Aging. *Metabolomics* **2021**, *17*, 9.
(68) Silva, R. E.; Baldim, J. L.; Chagas-Paula, D. A.; Soares, M. G.; Lago, J. H.; Goncalves, R. V.; Novaes, R. D. Predictive metabolomic signatures of end-stage renal disease: A multivariate analysis of population-based data. *Biochimie* **2018**, *152*, 14−30.
(69) Xia, J.; Bjorndahl, T. C.; Tang, P.; Wishart, D. S. MetaboMiner–semi-automated identification of metabolites from 2D NMR spectra of complex biofluids. *BMC. Bioinformatics* **2008**, *9*, 507.
(70) Guleria, A.; Misra, D. P.; Rawat, A.; Dubey, D.; Khetrapal, C. L.; Bacon, P.; Misra, R.; Kumar, D. NMR-based serum metabolomics discriminates Takayasu arteritis from healthy individuals: a proof-of-principle study. *J. Proteome Res.* **2015**, *14*, 3372−3381.
(71) Guleria, A.; Kumar, U.; Kumar, D.; Anuja, A. K.; Singh, M. K.; Sharma, P.; Agarwal, V.; Misra, R.; Gupta, L. NMR-based serum and muscle metabolomics for diagnosis and activity assessment in idiopathic inflammatory myopathies. *Anal. Sci. Adv* **2021**, 515−526.
(72) Gupta, L.; Guleria, A.; Rawat, A.; Kumar, D.; Aggarwal, A. NMR-based clinical metabolomics revealed distinctive serum metabolic profiles in patients with spondyloarthritis. *Magn. Reson. Chem.* **2020**, 85−98.
(73) Dona, A. C.; Kyriakides, M.; Scott, F.; Shephard, E. A.; Varshavi, D.; Veselkov, K.; Everett, J. R. A guide to the identification of metabolites in NMR-based metabonomics/metabolomics experiments. *Comput. Struct. Biotechnol. J.* **2016**, *14*, 135−153.
(74) Xia, J.; Sinelnikov, I. V.; Han, B.; Wishart, D. S. MetaboAnalyst 3.0-making metabolomics more meaningful. *Nucleic Acids Res.* **2015**, *43*, W251−W257.
(75) Chong, J.; Soufan, O.; Li, C.; Caraus, I.; Li, S.; Bourque, G.; Wishart, D. S.; Xia, J. MetaboAnalyst 4.0: towards more transparent and integrative metabolomics analysis. *Nucleic Acids Res.* **2018**, *46*, W486−W494.
(76) Xia, J.; Psychogios, N.; Young, N.; Wishart, D. S. MetaboAnalyst: a web server for metabolomic data analysis and interpretation. *Nucleic Acids Res.* **2009**, *37*, W652−W660.
(77) Jain, A.; Kumar, D.; Guleria, A.; Misra, D. P.; Zanwar, A.; Chaurasia, S.; Kumar, S.; Kumar, U.; Mishra, S. K.; Goel, R.; Danda, D.; Misra, R. NMR-Based Serum Metabolomics of Patients with Takayasu Arteritis: Relationship with Disease Activity. *J. Proteome Res.* **2018**, *17*, 3317−3324.
(78) Xia, J.; Wishart, D. S. Web-based inference of biological patterns, functions and pathways from metabolomic data using MetaboAnalyst. *Nat. Protoc.* **2011**, *6*, 743−760.
(79) Szymanska, E.; Saccenti, E.; Smilde, A. K.; Westerhuis, J. A. Double-check: validation of diagnostic statistics for PLS-DA models in metabolomics studies. *Metabolomics* **2012**, *8*, 3−16.
(80) Trygg, J.; Wold, S. Orthogonal projections to latent structures (O-PLS). *J. Chemom.* **2002**, *16*, 119−128.
(81) Eriksson, L.; Johansson, E.; Kettaneh-Wold, N.; Wold, S. *Introduction to multi-and megavariate data analysis using projection methods (PCA & PLS)*. Umetrics: Umea 1999,
(82) Xia, J.; Wishart, D. S. Metabolomic data processing, analysis, and interpretation using MetaboAnalyst. *Curr. Protoc. Bioinf.* **2011**, *34*, 14−10.
(83) Xia, J.; Wishart, D. S. Using MetaboAnalyst 3.0 for comprehensive metabolomics data analysis. *Curr. Protoc. Bioinf.* **2016**, *55*, 14−10.

https://doi.org/10.1021/acsomega.2c06469
ACS Omega 2023, 8, 7722−7737

(84) Rawat, A.; Misra, G.; Saxena, M.; Tripathi, S.; Dubey, D.; Saxena, S.; Aggarwal, A.; Gupta, V.; Khan, M. Y.; Prakash, A. 1H NMR based serum metabolic profiling reveals differentiating biomarkers in patients with diabetes and diabetes-related complication. *Diabetes Metab. Syndr.* **2019**, *13*, 290−298.
(85) Calle, M. L.; Urrea, V. Stability of Random Forest importance measures. *Briefings Bioinf.* **2011**, *12*, 86−89.
(86) Han, H.; Guo, X.; Yu, H. Variable selection using mean decrease accuracy and mean decrease gini based on random forest. *2016 7th ieee international conference on software engineering and service science (icsess)* 2016, 219−224.
(87) Quist, J.; Taylor, L.; Staaf, J.; Grigoriadis, A. Random forest modelling of high-dimensional mixed-type data for breast cancer classification. *Cancers* **2021**, *13*, 991.

https://doi.org/10.1021/acsomega.2c06469
ACS Omega 2023, 8, 7722−7737